Research Article | Vol. 29, No. 13 / 21 June 2021 / Optics Express 19998
Optics EXPRESS

Salient role of the non-Hermitian coupling for optimizing conditions in multiple maximizations of inter-cavity light transfer

HYEON-HYE YU,[1] SUNJAE GWAK,[1] HYUNDONG KIM,[1] JUNG-WAN RYU,[2] CHIL-MIN KIM,[1,3] AND CHANG-HWAN YI[1,2,4]

[1]Department of Emerging Materials Science, DGIST, Daegu 42988, Republic of Korea
[2]Center for Theoretical Physics of Complex Systems, Institute for Basic Science (IBS), Daejeon 34126, Republic of Korea
[3]chmkim@dgist.ac.kr
[4]yichanghwan@ibs.re.kr

Abstract: We reveal that non-Hermitian lossy couplings in an inter-cavity light transfer process are crucial for an optimum light transfer, unlike the prevailed belief. Our results turn out the fact that the light transfer can have multiple maxima following the increased inter-cavity distance. To validate this finding both in the weak and strong coupling regimes, we demonstrate our claim in the vicinity of the so-called exceptional point. We believe our results can contribute to realizing coupled-optical-cavity-based devices which is functional with an ultra-efficient light transfer, especially when the device scale is as small as the operation wavelength.

1. Introduction

Coupled optical cavities (COCs) have been of special importance for several decades because of their highly prospective applicability in broad photonic-integrated systems [1–4]. In particular, it has been demonstrated that coupled-resonator-optical-waveguides (CROWs) structure can provide controllable functionalities on photonic dispersions by means of a nearest-neighbor inter-resonator interaction [5]. Recent leading-edge technologies have shown that this coupled optical cavity system can also be utilized to realize even a slow light propagation [6] which is the key ingredient in many fascinating applications, such as optical delay lines [7,8], switches [9–11], memory [12,13], and quantum information process [14–17].

To accomplish these cavity-array-optical devices as desired, it is crucial first to account for an in-depth operating mechanism of an inter-cavity power transfer of light. Unfortunately, the clear condition for an efficient light transfer in inter-cavity interactions has not been well understood yet, even though its importance is as pivotal as the mode interaction itself. There have been a great number of works in a comprehensive range of physics focusing on resonant modes and their interactions in COCs, e.g., photonic-molecular states [18–21]. However, in those studies, still, the light transfer mechanism was not fully addressed and explained enough.

For the past several decades, the coupled-mode theory (CMT) has been intensively developed to study a light transfer in coupled systems, such as coupled waveguides [22–24], waveguides-coupled-ring resonators (bent waveguides) [25,26], and waveguide-coupled-cavities [27–30]. Since this CMT is based on the Maxwell's equation in lossless systems, the involved couplings naturally satisfy the conservative condition, i.e., two coupling coefficients are mutually complex-conjugates. Following this principal background, most of modeling studies dealing with various coupled systems use this conservative CMT. In most typical cases, the coupling coefficients are determined by a numerical fitting that forces real-numbered coupling coefficients or just by assuming complex-conjugate couplings for simplicity [31–35]. As a consequence, the effect of realistic lossy-couplings [36,37] has been often overlooked. These conventional lossless

#430778 https://doi.org/10.1364/OE.430778
Journal © 2021 Received 5 May 2021; revised 30 May 2021; accepted 31 May 2021; published 10 Jun 2021

Optics EXPRESS

couplings bring about a monotonic behavior of inter-cavity light transfer efficiency with respect to a coupling strength and shows no special properties noteworthy. We demonstrate, however, that an optimum condition for an inter-cavity light transfer can be obtained if we consider a non-conservative inter-cavity coupling process, which can be realized by implementing complex-numbered-coupling coefficients. As such coupling coefficients turn our effective Hamiltonian to be a fully non-Hermitian operator [36], we will refer to these coupling as non-Hermitian coupling throughout this work.

The effect of non-Hermitian coupling has attracted increasing attention in recent years. So far, a number of outstanding systems utilizing an inter-site non-Hermitian coupling have been proposed to realize fruitful features for applications, like an unidirectional light transport or a light trapping in a photonic lattice [38,39], photonic refrigeration [40]. In most of those newly suggested systems, artificially designed non-Hermitian couplings, for example, using the auxiliary resonators, mainly function to produce asymmetric coupling between two adjacent coupling sites. On top of the traditional formalism, recently, there have been notable trials to improve the coupled-mode theory implementing these non-conservative situations [41–43]. For instance, non-Hermitian coupling-induced abnormal dispersion relations, as well as nontrivial group velocities, in CROWs and in photonic lattice have been demonstrated successfully [37,44]. While some of the importance of complex-valued coupling coefficients were addressed in those works too, yet the associated impact on light transfer efficiency was not explored clearly up to date. In this motivation, we will reveal the explicit effect of non-Hermitian coupling on the inter-cavity light transfer in relation to the full non-Hermitian resonance dynamics of COC.

To investigate an inter-cavity light transfer, we model two coupled optical microdisks by means of the temporal coupled-mode theory (TCMT) [23]. The coupling coefficients, which are the core variables in TCMT, are calculated in terms of passive mode overlaps obtained by the boundary element method (BEM) [45,46]. The inter-cavity light transfer prediction established upon this BEM-TCMT hybrid method is confirmed by numerical results of the time-dependent experiments carried out through the finite-difference-time-domain (FDTD) solver. In demonstrations, a transmittance ($\equiv T$) is obtained as a function of an input frequency ($\equiv \omega$) and an inter-cavity distance ($\equiv D$). Our results show that T can have multiple maxima implying the fact that the optimal-coupling modes can alternate between the two interacting modes as a function of D. More surprisingly, it is revealed that a strongly oscillating coupling strength can result in a non-trivial excessive light transfer even for a long distant coupling. By analyzing these results, it turns out that an optimum light transfer location in (ω, D)-space is deeply associated with a non-Hermitian coupling effect which becomes particularly prominent when the system size decreases (or equivalently, the frequency is decreased). We believe our findings will perform a crucial role in realizing ultra-efficient coupled-optical-cavity systems, especially when the device size is as small as sub-wavelength-scale in future optoelectronic devices.

2. Strong and weak coupling of super-modes in a coupled non-identical cavity

Our coupled optical microcavity system consists of two non-identical dielectric microdisks that have different radii of $\{r_1, r_2\}$ and an inter-cavity distance d_0, as shown in the inset of Fig. 1(b). The refractive index of the inside and the outside of the cavity is set to be $n = 2.0$ and $n = 1.0$, respectively. In the present paper, our analyses are focused on, so-called, whispering gallery modes (WGMs) having a transverse magnetic (TM) polarization $(0, 0, E_z)$, where E_z is the electric field polarized along z-direction (perpendicular to the microdisk plane). In this configuration, optical modes are computed by solving the Helmholtz equation, $-\nabla^2\psi(r) = n^2(r)k^2\psi(r)$ accompanied by a time-harmonic field assumption, $\psi \sim e^{-i\omega t}$, where k is a complex-numbered-wavenumber in a vacuum and $i^2 = -1$.

In Figs. 1(a) and (b), real and imaginary parts of these solutions, $k_\pm$, obtained by BEM are given as a dimensionless value, kr_2, in the parameter space $(R, D) \equiv (r_1/r_2, d_0/r_2)$. The

Optics EXPRESS

figures demonstrate a characteristic structure of the Riemann surface around the branch point, the so-called exceptional point of super-mode in COC [47]. The occurrence of the exceptional point is a special feature of the non-Hermitian system, at which both the eigenvalues and the corresponding eigenstates coalesce simultaneously [48,49]. Tracing eigenvalues on the obtained Riemann surface, we can identify two distinct coupling regimes: in the strong (weak) coupling regime, the avoided resonance crossings occur in real (imaginary) parts of solutions, while the imaginary (real) parts do cross [47,49]. Note that this branching behavior does not occur in coupled identical disks: degenearacies of the real and imaginary parts of eigenvalues are immediately lifted as the inter-disk coupling is introduced and never cross each other as D decreases [47]. In the present manuscript, we will cover the more general case of coupled nonidentical disk systems.

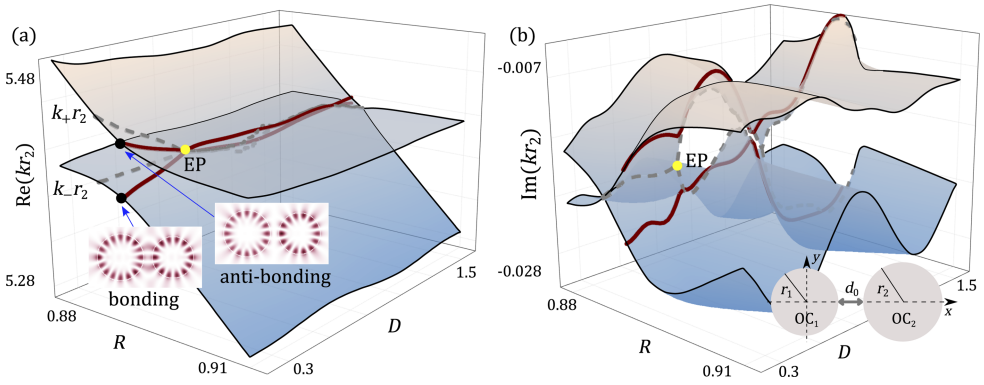

Fig. 1. (a) and (b) are the Riemann surfaces of the real and imaginary parts of $k_\pm r_2$ obtained by BEM in the parameter space $(R, D) \equiv (r_1/r_2, d_0/r_2)$. The EP at the branch point of the surface is marked in yellow dot, and $k_\pm r_2$ values of our interest are represented in thick brown curves. The system configuration is shown in the inset of (b), and the representative mode patterns of a bonding and an anti-bonding mode are shown in the inset of (a).

The evolution of complex-eigenvalues on the Riemann surfaces in 2-dimensional parameter space (R, D) implies that the coupling strength can vary depending on either R or D. That is, while the overall coupling strength between two interacting modes (localized on separate cavities) grows as D gets smaller, the most maximized coupling takes place at a specific R-value, $R = 0.891$, where a detuning between k_+ and k_- is minimized so that the resonant frequencies of two isolated modes are matched to one another [50]. We will focus on the inter-cavity light transfer depending on D at this specific $R = 0.891$ throughout this work.

3. Coupled mode equation formalism for light tranfer in COC

Even though the passive mode calculations carried out in the previous section can give lots of important information on fundamental mode structures in parameter space, the light transfer characteristics cannot be captured in those computations. Hence, in this section, we will bring this light transfer problem into the coupled-mode theory framework constructed on the basis of those passive mode calculations.

The coupling of two modes confined in separate non-identical optical cavities $(\mathrm{OC}_1, \mathrm{OC}_2)$ can be described employing the temporal-coupled-mode-theory (TCMT) equations, as follows:

$$\begin{aligned} \frac{da_1}{dt} &= -i\omega_1 a_1 - g_1 a_1 - i\mu_{12} a_2 \\ \frac{da_2}{dt} &= -i\omega_2 a_2 - g_2 a_2 - i\mu_{21} a_1 + \sqrt{g_s} S_{\mathrm{in}} \,, \end{aligned} \tag{1}$$

Optics EXPRESS

where a_j, ω_j, g_j, μ_{ij} are the mode amplitude, the resonance frequency, the decay rate, and the coupling coefficient, respectively. The above coupled-mode equations imply that the input power, $S_{\text{in}} = S_0 e^{-i\omega t}$, coupled into the OC_2 with a rate of g_s transfers to the OC_1 through the coupling rate of μ_{ij}. At the steady-state, $|a_1|$ and $|a_2|$ become the constant in time and can be written as

$$\begin{aligned} a_1^0(\omega) = |a_1| &= \left| \frac{-i\mu_{12}\sqrt{g_s}S_0}{\mu_{12}\mu_{21} - (\omega - \omega_1 + ig_1)(\omega - \omega_2 + ig_2)} \right| \\ a_2^0(\omega) = |a_2| &= \left| \frac{-i\sqrt{g_s}S_0(\omega - \omega_1 + ig_1)}{\mu_{12}\mu_{21} - (\omega - \omega_1 + ig_1)(\omega - \omega_2 + ig_2)} \right|, \end{aligned} \tag{2}$$

for which a_j^0 can be determined when the coupling coefficients, μ_{ij}, are fixed. In common treatments of these couplings, they are just ones of the varying parameters of modelings that assume the values of μ_{ij} are real and symmetric, i.e., $\mu_{12} = \mu_{21} \in \mathbb{R}$. In the present work, we will follow the methods in [46] using the overlap of the modes to calculate μ_{ij} explicitly. It is emphasized that this approach gives more precise results than the traditional spatial coupled mode theory, for this approach uses the exact "coupled-modes" instead of using only the "isolated-modes" of which each one is localized on the isolated cavities OC_1 and OC_2.

3.1. Obtaining coupling strengths in an effective Hamiltonian

The key quantities in investigating the light transfer property in the COC systems through TCMT are the unknown coupling coefficient, μ_{ij}, in Eq. (2) since others can be given by the isolated basis modes. The coupling of two isolated modes can be written as a two-level system with an effective Hamiltonian, $\mathbf{H}_{\text{eff}}$,

$$\mathbf{H}_{\text{eff}}\mathbf{c}^{\pm} = \begin{pmatrix} \omega_1 - ig_1 & \mu_{12} \\ \mu_{21} & \omega_2 - ig_2 \end{pmatrix} \begin{pmatrix} c_1^{\pm} \\ c_2^{\pm} \end{pmatrix} = \lambda_{\pm} \begin{pmatrix} c_1^{\pm} \\ c_2^{\pm} \end{pmatrix}, \tag{3}$$

where $c_j^{\pm} \in \mathbb{C}$ are elements of the eigenvector and $\lambda_{\pm} \equiv \omega_{\pm} - ig_{\pm}$ are complex-numbered eigenvalues with $\omega_{\pm},\ g_{\pm} \in \mathbb{R}$. In the vicinity of an interaction point of two modes (i.e., $\omega_+ \sim \omega_-$), the coupled modes can be constructed in terms of $c_j^{\pm}$ in Eq. (3), as $E_{\pm}(\mathbf{r}) = [c_1^{\pm}E_1(\mathbf{r}) + c_2^{\pm}E_2(\mathbf{r})]$, where E_j are the isolated-basis modes and $E_{\pm}$ are the coupled modes. Under the bi-orthogonal normalization of modes, $\int n_i^2(\mathbf{r})E_i(\mathbf{r}) \cdot E_j(\mathbf{r})\, d\mathbf{r} = \delta_{ij}$ [51], we can obtain $c_j^{\pm}$ by computing the overlap integrals between the coupled modes and the isolated modes:

$$c_j^{\pm} = \int n_j^2(\mathbf{r})E_j(\mathbf{r}) \cdot E_{\pm}(\mathbf{r})\, d\mathbf{r}\,. \tag{4}$$

Defining $\lambda_j = \omega_j - ig_j$ for the diagonal elements in the unperturbed Hamiltonian, all elements in the effective Hamiltonian can be calculated by solving

$$\begin{pmatrix} \lambda_1 - \lambda_{\pm} & \mu_{12} \\ \mu_{21} & \lambda_2 - \lambda_{\pm} \end{pmatrix} \begin{pmatrix} c_1^{\pm} \\ c_2^{\pm} \end{pmatrix} = 0\,, \tag{5}$$

with the known values of $\lambda_{\pm} = k_{\pm}c$ (with $k_{\pm}$ in Fig. 1) and $c_j^{\pm}$ [46]. Now, we can obtain a_j^0 in Eq. (2), as a function of an input frequency ω, since all other values necessary for computing it are prepared.

4. Multiple maximizations of inter-cavity light transfer efficiency

Given the values of a_j^0, we can obtain the light transfer efficiency from the source cavity, OC_2, to the receiver cavity, OC_1, by defining the transmittance $T \equiv |a_1|$. Figure 2(a) shows T at $R = 0.891$

Optics EXPRESS

as a function of D and $k_{\text{in}} \equiv \omega r_2/c$, which is a wavenumber of the input frequency scaled by r_2. In the figure, two counter-intuitive important features are discovered: (1) It turns out that there are multiple local maxima of transmittance along the parametric variation of D, and (2) no mirror-reflection symmetry is found in the transmittance spectra with respect to a certain value of k_{in}. These two findings are strongly associated with the non-Hermitian coupling of modes in COC, as explained in the following. The splitting ($\equiv \Delta\lambda$) of degenerated resonant frequencies ($\equiv \lambda_0 = \lambda_1 = \lambda_2$) of two interacting modes are directly proportional to the coupling ($\equiv V$) of the two modes as

$$\lambda_{\pm}=\lambda_0 \pm |V| \iff \Delta\lambda = |\lambda_+ - \lambda_-| = 2|V| \,,$$

based on the typical Hermitian coupling assumption, i.e., $V_{1\to2} = V^*_{2\to1}$. The two resulting coupled modes are a symmetric or an anti-symmetric superposition of two isolated basis modes. Thus, there must be no preference between the two modes in the inter-cavity light transfer process. In addition, it seems reasonable for us to expect that the strength of this coupling might decrease exponentially and monotonically, when the distance between the two cavities increases, i.e., increasing D. Hence, it is natural to look forward to a monotonic-descending and mode-symmetric light-transfer rate, as well. Indeed, if we set the coupling coefficient to be real-symmetric, i.e., $\mu_{12} = \mu_{21} \in \mathbb{R}$ in Eq. (2), which decreases exponentially with increasing D, we can obtain a quickly diminishing (i.e., exponential decreasing) Λ-shaped (i.e., mode-symmetric) transmittance when D increases, as shown in the inset of Fig. 2(a).

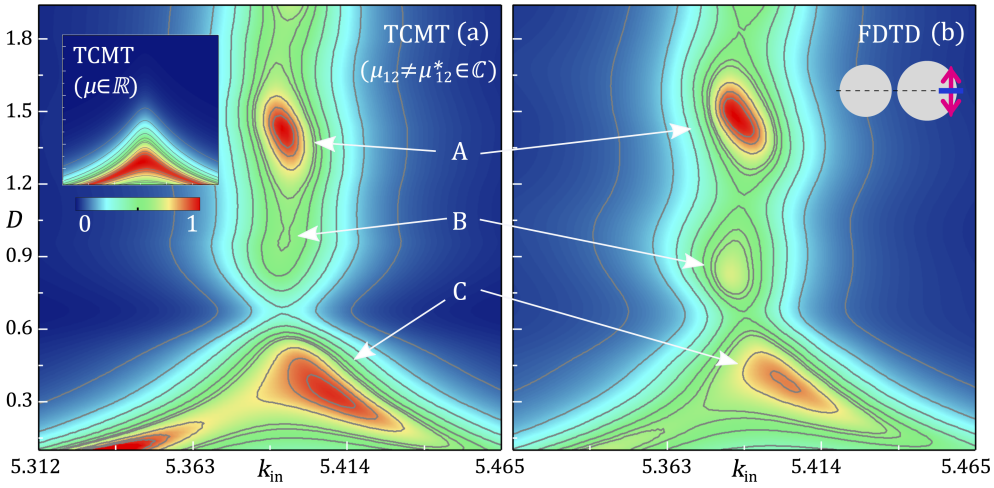

Fig. 2. (a) and (b) are T at $R = 0.891$ obtained in (k_{in}, D)-space by TCMT and FDTD respectively. The locations of local maxima of T are marked as point-A, B, and C. The inset of (a) is T obtained by real-numbered exponentially decaying coupling coefficients, and the inset of (b) shows the system configuration we used in FDTD simulation. The arrows of the latter inset represent the location and the propagation directions of the input source.

However, as we can see in Fig. 2(a), this expectation is totally not the case at all: our TCMT results of T obtained without the Hermitian-like coupling assumption have multiple peaks and no mode-symmetric features as D varies. The underlying factors causing these unexpected features of the light transfer behavior in COC will be discussed step-by-step in the following.

4.1. *Time-dependent numerical experiments of light transfer in COC*

To verify our results obtained in the previous sections, we perform the time-dependent numerical simulations using the finite difference time domain (FDTD) method. In Fig. 2(b), we can clearly see that the FDTD results more likely to resemble our TCMT results instead of the exponentially

Optics EXPRESS

decaying and symmetric-balanced transmittance. In fact, from the regularity viewpoint, the FDTD results show even more substantial fluctuations in the transmittance spectra than the one of our TCMT results. Therefore, the FDTD results strongly support our TCMT-based prediction of the non-regular light transfer, clarifying that the inter-cavity light transfer in the COC systems should be described by the non-Hermitian couplings achieved automatically in our TCMT calculations. Note that for our FDTD simulations, we locate the input mode source inside the OC_2 as depicted in the inset of Fig. 2(b) so that $g_s = 1$ in Eq. (2), and obtain the energy density inside the OC_1 at the steady-state,

$$|a_j(k_{\rm in})| \equiv \left\{ \frac{1}{2A_j} \int_{{\rm OC}_j} \left[n^2(\mathbf{r}) |E_j(\mathbf{r})|^2 + |B_j(\mathbf{r})|^2 \right] \, d\mathbf{r} \right\}^{1/2} ,$$

which is the same quantity as $|a_j|$ in Eq. (2). Note further that the results of our TCMT modeling and simulations shown in Figs. 2(a) and (b) have comparable intensities even when $D/\lambda_{\rm avg}>1$, where the average wavelength of $k_{\rm in}$ is $\lambda_{\rm avg}/r_2 \sim 1.16$.

5. Coupling strength vs lifetimes of modes in multiple maxima of light transfer

From now on, we will demonstrate that the asymmetric multiple maximizations of the light transmittance in COC are a consequence of the non-Hermitian coupling effects. More precisely, we will show that the maxima of T in Figs. 2 and 3 cannot be explained if we take into account the coupling strength $|\mu_{ij}|$ or the lifetime, $\tau_\pm \equiv 1/g_\pm$, of the coupled modes individually, but it is only possible when the multiplication of them is considered. By assuming that each resonant peak of the coupled modes is a single Lorentzian peak,

$$T \sim \frac{\mu_c}{(\omega - \omega_\pm)^2 + g_\pm^2} , \quad \omega,\ \omega_\pm,\ g_\pm \in \mathbb{R} , \tag{6}$$

we can easily see that $T \propto \mu_c \tau_\pm^2 (\equiv \eta_\pm)$ at the resonance, i.e., $\omega = \omega_\pm$, where $\omega_\pm$ and $g_\pm$ are the resonant frequency and the decay-rate of the coupled modes. Here, we defined $\mu_c \equiv |\mu_{12}|\sqrt{g_s} S_0$, where $\sqrt{g_s}$ and S_0 are constants. To begin with, we project the obtained transmittance in Fig. 2 onto D-axis by integrating them as $T_{\rm tot}(D) \equiv \max(T_{\rm tot})^{-1} \int_{k_{\rm in}} T(k, D) {\rm d}k$, so that we can investigate the overall D-dependent light transmittance in the considered range of $k_{\rm in}$. We can confirm once again in Fig. 3(a) that the CMT results using μ_{ij} obtained by the wave overlap reproduce the FDTD results successfully, while the CMT result using the real-numbered-exponentially-decaying μ_{ij} fails. Note that the indiscernible local maximum of A in Fig. 3(a) is an artificial effect caused by integrating two peak contributions in the strong coupling regime D<0.6. The obtained $T_{\rm tot}$(D) is analyzed by a D-dependent coupling strength $|\mu_{ij}|$ shown in Fig. 3(c). In the figure, two distinct regions of different D-dependent slopes that are connected across the transition valley region (marked by the vertical shading band) are revealed. In the region (I) (D<0.55), $|\mu_{ij}|$ decreases exponentially as if it follows a common evanescent coupling [52]. Afterward, in (II) (D>0.75), $|\mu_{ij}|$ revives again and starts to exhibit a mild oscillation. Meanwhile, there is a sudden slope change around $D \sim 0.565$ in the transition region which is found to coincide with the exceptional point $D_{\rm EP}$ dividing the strong and the weak coupling regimes. From $D_{\rm EP}$, $|\mu_{ij}|$ decreases with a sub-exponential decaying rate until it reaches the minimum value. Note that while explicit analyses to understand the role of the exceptional point on this abrupt change of the coupling strength are necessary, this agenda is beyond the scope of the present works; we leave this topic and postpone it to the more elaborated next proceeding works elsewhere.

5.1. Light transfer in a strong coupling regime

We first focus our attention on the transmittance in the strong coupling regime (I). As we already clarified, the overall trend of T features a broken mirror symmetry [see Figs. 2(a) and (b)]. This

Optics EXPRESS

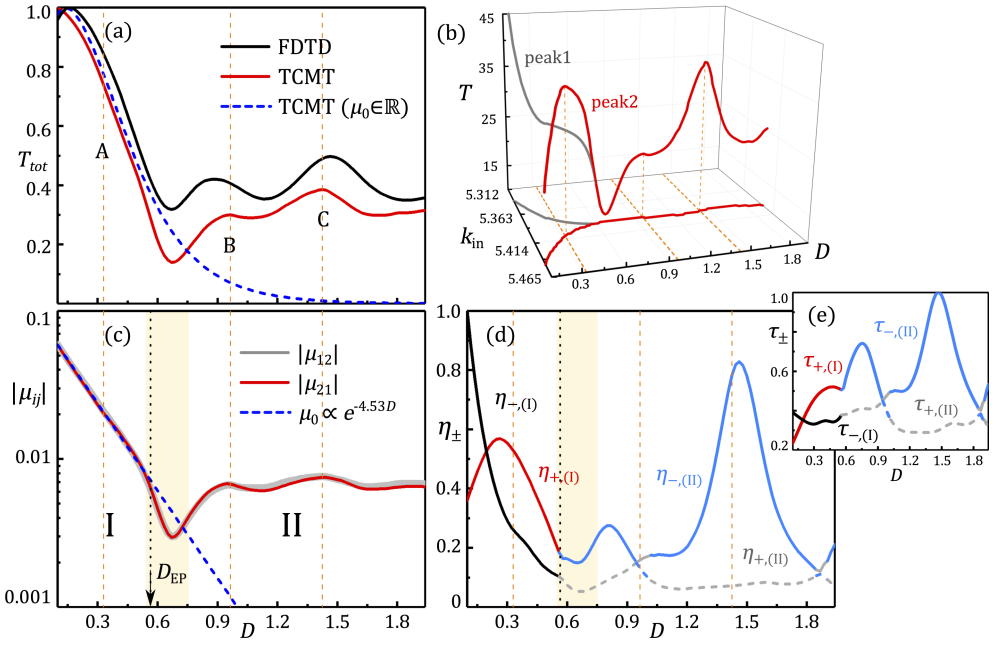

Fig. 3. $T_{\mathrm{tot}}(D)$ obtained by FDTD and TCMT are shown in (a). The black, red, blue-dashed curves are the results of FDTD, TCMT with μ_{ij} obtained by wave overlap, and the result of TCMT with exponentially decaying $\mu_{ij} = \mu_0 \in \mathbb{R}$. The peak values of T in Fig. 2(a) are shown in (b). (c) shows the absolute values of μ_{ij} obtained by wave overlap at $R = 0.891$ as a function of D, and μ_0 which is obtained by exponential curve fitting of the $|\mu_{12}|$ in the region of D<0.5. (d) and (e) show $\eta_{\pm}$ and $\tau_{\pm}$, which are obtained by BEM, respectively. The multiple local maxima of T in Fig. 2(a) occur at $D = 0.33, 0.965, 1.425$, and these locations are marked by vertical dashed lines.

characteristic is particularly prominent in the region (I) due to the highly selective preferences of modes in the light transfer process [see Fig. 3(b)]: the bonding mode (peak1) dominates T at D<0.2 and the anti-bonding mode (peak2) at D>0.2. Moreover, since the latter one reduces again when we further increase D in the region (I), it exhibits a peak structure at A, as is shown in Fig. 2. This D-dependent shift of the dominant light transfer channel is brought by a sequential switching of the longer-lived resonant mode.

If this highly irregular T is compared to the coupling strength $|\mu_{ij}|$ in the region (I), the coupling can be seen as regular along the D variation, as shown in Fig. 3(c). In the figure, $|\mu_{ij}|$ decreases exponentially and monotonically for increasing D. This exponential decay is well-fitted by an exponent (~ -4.53) (see blue-dotted curve). At the same time, since the coupling strength has no mode-dependence, the coupling effect should be reflected equally in both the bonding and the anti-bonding modes. Thus, if we suppose $|\mu_{ij}|$ alone operates in the light transfer process, we can hardly expect a mode-dependent transmittance difference. In other words, there are more factors giving rise to the observed irregular transmittance, which we have to uncover.

Through our investigations, it turns out that the crucial factor that brings an asymmetricity of T in the region (I) is the lifetime of a coupled mode, which is shown in Fig. 3(e). As we can see in Fig. 3(d), a factor $\eta_{\pm}$ which is a multiplication of the coupling strength and the square of mode lifetime ($\equiv \mu_c \tau_{\pm}^2$), explicitly reveals all peak structures of A in the region (I), as well as B and C in the region (II). In the figure, the black curve corresponding to T of the bonding mode decreases monotonically as D increases, while the red curve of the anti-bonding mode makes a local maximum around the point A. Here, slight mismatches in the peak positions come

Optics EXPRESS

from the difference between a_1^0 in Eq. (2) and the simplified Lorentzian expression in Eq. (6). Nevertheless, our claim that a dominant factor that makes the peak structure of T along the D variation is $\eta_\pm$ is valid consistently. Based on those observations, we can argue that the most important quantity that makes the asymmetricity of T in the region (I) is the lifetime of the modes which varies drastically with D. The essential mechanism that makes this drastic variation of the lifetimes is the non-Hermitian coupling between two basis modes, which will be explained later in the proceeding sections.

5.2. Light transfer in a weak coupling regime

One of the interesting observations in Figs. 2(a) and (b) is that the significant amount of the transmittance T (i.e., light transfer) can take place even far beyond the evanescent regime, more strictly speaking, in the weak coupling regime of (II). In addition, this revived transmittance T oscillates along the D variation and exhibits multiple numbers of local maxima. Even more surprisingly, the transmittance at C in the region (II) exceeds the one at A in the region (I).

First, the significant amounts of T in the region (II) are induced by the coupling strength revival which happens after the transition region. This fact is proven by giving the counter exemplification of the exponentially decaying transmittance [blue-solid curve in Fig. 3(a)] which is obtained by using the artificial coupling coefficients $\mu_{ij} \leftarrow \mu_0$ [blue-dotted fitting curve in Fig. 3(c)]. In short, if the exponential decaying of the coupling strength in the region (I) continues even in the region (II), rather than the reviving, the transmittance in the region (II) will practically disappear.

Second, the multiple local maxima of T in the region (II) originate from the oscillating feature of the revived coupling strength, as we can confirm it by the perfectly matching local maxima of B and C with $|\mu_{ij}|$ [see Figs. 3(a) and (c)]. Nonetheless, this oscillating μ_{ij} is not sufficient when it comes to the largest maximum of T at C, since $|\mu_{ij}|$ in the region (II) cannot exceed any values in the region (I). In fact, this largest value of T is induced by the largest lifetimes of modes. Especially, τ_- around the point C shows an extremum value which is about 2 times larger than the $\tau_\pm$ in the region (I). Moreover, since each of the coupled mode contributions in T is summed up in the region (II) due to the negligible frequency splitting between the two modes in this region, we can obtain the highest value of the transmittance at C, not A. Here, we have to emphasize that studies for inter-cavity mode interactions beyond the evanescent regime have appeared in a very limited number of previous works, e.g., in [53,54], to the best of our knowledge. However, even in these studies, elaborated and explicit findings on the interplaying effects of the coupling strength variations and the inter-cavity light transfer were absent; those studies are more focused on obtaining efficient long distant couplings using directional-emitting deformed cavities and analyzing eigenmodes.

5.3. Effect of the non-Hermitian couplings in light transfer

So far, we have demonstrated that the coupling strength between the basis modes and the lifetime of the coupled modes have a decisive effect on the inter-cavity light transfer process. Particularly, the large variations of $\tau_\pm$ have turned out to be a key factor that can bring the multiple local maxima and asymmetricity in the light transfer. In fact, these large variations of $\tau_\pm$ are a direct consequence of the "non-Hermitian" coupling between two isolated basis modes, as we can see below.

By definition, the lifetime $\tau_\pm = 1/g_\pm$ can be determined by obtaining the eigenvalues of the effective Hamiltonian in Eq. (3), as follows:

$$\tau_\pm = \left| \mathrm{Im}\left[\frac{\lambda_1 + \lambda_2}{2} \pm \frac{1}{2}\sqrt{(\lambda_1 - \lambda_2)^2 + 4\mu_{12}\mu_{21}} \right]^{-1} \right|. \tag{7}$$

Optics EXPRESS

Now, since the term $\pm\sqrt{(\lambda_1-\lambda_2)^2+4\mu_{12}\mu_{21}}/2$ in Eq. (7) determines the splitting of the real and imaginary parts of eigenvalues, only the full-complex-valued μ_{ij} in Fig. 4(c) can reproduce the correct $\tau_\pm$ and, in turn, the correct T. Note that the non-Hermitian coupling, $\mu_{12} \neq \mu_{21}^*$, in Fig. 4(c) makes $\mathbf{H}_{\text{eff}}$ to be fully non-Hermitian and enables the external coupling through an environment [36]. Note that the observed balanced couplings, $\mu_{12} \approx \mu_{21}$, might be ascribed to the evenly distributed two eigenmodes on both disks, at $R = 0.891$, since the similar mode overlap coefficients, $c_1^\pm \approx c_2^\pm$, in Eq. (4) can lead to balanced mode couplings.

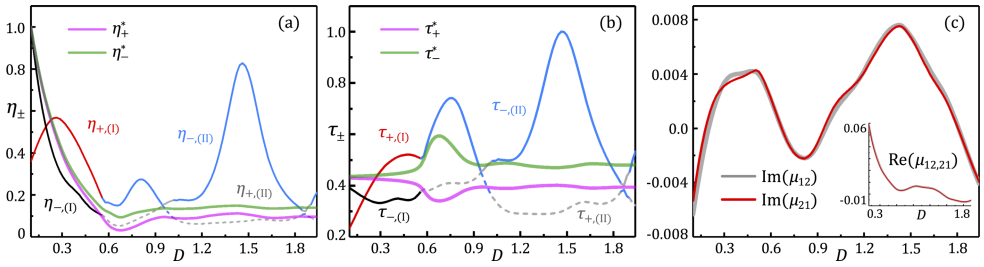

Fig. 4. $\eta_\pm^*$ and $\tau_\pm^*$ obtained by "Hermitian-like" coupling, $\mu_{ij} \leftarrow |\mu_{ij}|$ are shown in pink and green-colored curves in (a) and (b) respectively. The $\eta_\pm$ and $\tau_\pm$ with exact μ_{ij} in Figs. 3(d) and (e) are redrawn in (a) and (b) for comparison. In (c), the imaginary parts of full-complex-numbered coupling coefficients are shown, and the real parts of them are shown in the inset.

On the other hand, if those couplings in the Hamiltonian are assumed to be "Hermitian-like" corresponding to the lossless coupling (i.e., there is no loss in the coupling process), $\mu_{12} = \mu_{21}^*$ must be satisfied [50]. Then, since the square root term on the right-hand side in Eq. (7) becomes $\pm\sqrt{(\lambda_1-\lambda_2)^2+4|\mu_{12}|^2}/2$ for this coupling condition, it can only give rise to the real-numbered shift. That is, $\tau_\pm$ deduced under the lossless coupling never can result in the correct T: it cannot reproduce the exact eigenvalues, especially the lifetime of eigenmodes. This fact can be clearly verified through $\eta_\pm^*$ and $\tau_\pm^*$ in Figs. 4(a) and (b), which are obtained with $\mu_{ij} \leftarrow |\mu_{ij}|$. Therefore, we can conclude that the most essential ingredient giving rise to those all complicated but interesting features in the inter-cavity light transfer characteristics are raised from the non-Hermitian coupling effects.

5.4. *Larger cavity system case*

As a final remark, we examine the validity of our claim for the higher input frequencies case of $k_{\text{in}} \sim 8.784$ in a slightly different (R=0.93685) system from the ones studied so far. This frequency and the parameter are chosen in order to investigate the light transfer around the exceptional point. The transmittance obtained by BEM-TCMT hybrid approach is given in Fig. 5(a), and as in the previous case of the lower frequency, the divisions of the evanescent coupling regime [region (I)], the transition regime, and the long distant coupling regime [region (II)] are obviously visible in Fig. 5(b). Also, the peak structures of T in Fig. 5(a) are well-explained by $\eta_\pm$ in Fig. 5(c) in both the strong (I) and the weak coupling (II) regimes. In region (I), T of the anti-bonding mode in Fig. 5(a) is higher than the one of the bonding mode when $\eta_\pm$ of the anti-bonding mode (red-solid) is higher than that of the bonding mode (black-solid), and vice versa. Again, in region (II), the blue and gray curve in Fig. 5(c) also shows well-matched results with T at a weak coupling regime.

Despite the evident similarity in the overall trend of the inter-cavity light transfer behaviors, some notable differences are observed: (1) the higher frequency results in Figs. 5(a)-(c) seem more likely to follow the exponential decaying of the transmittance (i.e., the transmittance quenched relatively quickly). (2) There is no considerable oscillation of T or $\eta_\pm$ in Fig. 5(c), unlike

Optics EXPRESS

the previous case in Fig. 4(a). These deviating behaviors (especially the significantly reduced oscillation of T) in this higher frequency example, in comparison with the lower frequency case, is also associated with the non-Hermitian coupling effect: As the mode-confinement inside a cavity at the higher frequency is enhanced, the openness of a mode to the environment is decreased [55,56] so that the effect of the non-Hermitian coupling, which originates from the openness of modes, decreases, as well. Therefore, we can expect that the T behaviors will resemble the results of the Hermitian coupling assumption as the frequency is getting more and more increased, i.e., $\mu_{ij} \approx |\mu_{ij}|$ as $kr_2 \gg 1$. This fact also can be seen by comparing Fig. 4(a) and Fig. 5(c).

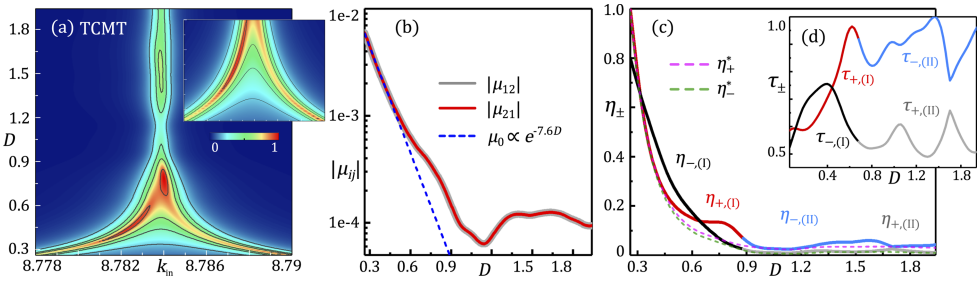

Fig. 5. T obtained in larger cavity system with $k_{in} \sim 8.784$ at $R = 0.93685$ are shown in (a). T in D<0.6 are shown as enlarged figure in the inset. (b) shows the absolute values of μ_{ij} obtained by wave overlap as a function of D, and μ_0 which is obtained by exponential curve fitting of the $|\mu_{12}|$ in the region of D<0.5. (c) and (d) show $\eta_\pm$ and $\tau_\pm$, calculated by BEM, respectively. The $\eta_\pm^*$ obtained by "Hermitian-like" coupling, $\mu_{ij} \leftarrow |\mu_{ij}|$ are also shown in (c) with pink and green-dashed curves.

6. Conclusion

To conclude, we have shown that an inter-cavity light transfer should be described in terms of a non-conservative mode interaction instead of a common conservative coupling approximation. As a consequence of these non-Hermitian coupling effects, the light transfer can have multiple optimum values of external parameters in a coupled optical microcavity system. These multiple maxima of the light transfer have not been discovered under the common Hermitian coupling approximation.

The effects of the non-Hermitian coupling are valid in both the weak and the strong coupling regime separated by the so-called exceptional points on the Riemann surface. In the strong coupling regime, when an inter-cavity distance is relatively small, the mode showing maximum light transfer switches between a bonding and an anti-bonding mode depending on the distance between the cavities. As the inter-cavity distance increases, the coupling regime changes to the weak coupling one, and the light transfer reveals several numbers of maximum peaks.

We have demonstrated that all these observed inter-cavity light transfer characteristics are brought by the oscillating coupling strength as well as the oscillating lifetime of the resulting coupled modes. Both of these two factors are the consequences of the non-Hermitian coupling which implies a non-conservative coupling process operating through the environment. Our findings and claims are benchmarked in a higher frequency regime as well, and reasonable results are obtained, which is consistent with the results of the lower frequency regime.

This work provides the explicit and exact way of analyzing the inter-cavity light transfer of the coupled cavity systems, especially for the devices in sub-wavelength scale. Thus, we believe that our findings can contribute to a wide range of applications implementing sub-wavelength optoelectronic coupling devices.

Funding. Institute for Basic Science (IBS-R024-D1); Korea Evaluation Institute of Industrial Technology (20012487).

Optics EXPRESS

Disclosures. The authors declare no conflicts of interest.

Data Availability. Data underlying the results presented in this paper are not publicly available at this time but may be obtained from the authors upon reasonable request.

References

1. W. Bogaerts, D. Pérez, J. Capmany, D. A. B. Miller, J. Poon, D. Englund, F. Morichetti, and A. Melloni, "Programmable photonic circuits," Nature **586**(7828), 207–216 (2020).
2. X. Xue, X. Zheng, and B. Zhou, "Super-efficient temporal solitons in mutually coupled optical cavities," Nat. Photonics **13**(9), 616–622 (2019).
3. H. Zhao, X. Qiao, T. Wu, B. Midya, S. Longhi, and L. Feng, "Non-hermitian topological light steering," Science **365**(6458), 1163–1166 (2019).
4. B. He, L. Yang, X. Jiang, and M. Xiao, "Transmission nonreciprocity in a mutually coupled circulating structure," Phys. Rev. Lett. **120**(20), 203904 (2018).
5. S. Mookherjea and A. Yariv, "Coupled resonator optical waveguides," IEEE J. Sel. Top. Quantum Electron. **8**(3), 448–456 (2002).
6. F. Morichetti, C. Ferrari, A. Canciamilla, and A. Melloni, "The first decade of coupled resonator optical waveguides: bringing slow light to applications," Laser Photonics Rev. **6**(1), 74–96 (2012).
7. M. Hafezi, E. A. Demler, M. D. Lukin, and J. M. Taylor, "Robust optical delay lines with topological protection," Nat. Phys. **7**(11), 907–912 (2011).
8. F. Xia, L. Sekaric, and Y. Vlasov, "Ultracompact optical buffers on a silicon chip," Nat. Photonics **1**(1), 65–71 (2007).
9. K. Mukherjee and P. C. Jana, "Controlled optical bistability in parity-time-symmetric coupled micro-cavities: Possibility of all-optical switching," Phys. E **117**, 113780 (2020).
10. D. Leykam, S. Mittal, M. Hafezi, and Y. D. Chong, "Reconfigurable topological phases in next-nearest-neighbor coupled resonator lattices," Phys. Rev. Lett. **121**(2), 023901 (2018).
11. S. Pereira, P. Chak, and J. E. Sipe, "Gap-soliton switching in short microresonator structures," J. Opt. Soc. Am. B **19**(9), 2191–2202 (2002).
12. M. Zhang, C. Wang, Y. Hu, A. Shams-Ansari, T. Ren, S. Fan, and M. Lončar, "Electronically programmable photonic molecule," Nat. Photonics **13**(1), 36–40 (2019).
13. H. Takesue, N. Matsuda, E. Kuramochi, W. J. Munro, and M. Notomi, "An on-chip coupled resonator optical waveguide single-photon buffer," Nat. Commun. **4**(1), 2725 (2013).
14. J. W. Silverstone, D. Bonneau, J. L. O'Brien, and M. G. Thompson, "Silicon quantum photonics," IEEE J. Sel. Top. Quantum Electron. **22**(6), 390–402 (2016).
15. S. Mittal, E. A. Goldschmidt, and M. Hafezi, "A topological source of quantum light," Nature **561**(7724), 502–506 (2018).
16. A. Blanco-Redondo, B. Bell, D. Oren, B. J. Eggleton, and M. Segev, "Topological protection of biphoton states," Science **362**(6414), 568–571 (2018).
17. X. Guo, C.-L. Zou, H. Jung, and H. X. Tang, "On-chip strong coupling and efficient frequency conversion between telecom and visible optical modes," Phys. Rev. Lett. **117**(12), 123902 (2016).
18. M. Bayer, T. Gutbrod, J. P. Reithmaier, A. Forchel, T. L. Reinecke, P. A. Knipp, A. A. Dremin, and V. D. Kulakovskii, "Optical modes in photonic molecules," Phys. Rev. Lett. **81**(12), 2582–2585 (1998).
19. S. V. Boriskina, "Coupling of whispering-gallery modes in size-mismatched microdisk photonic molecules," Opt. Lett. **32**(11), 1557–1559 (2007).
20. C. Yang, Y. Hu, X. Jiang, and M. Xiao, "Analysis of a triple-cavity photonic molecule based on coupled-mode theory," Phys. Rev. A **95**(3), 033847 (2017).
21. N. Caselli, F. Intonti, F. La China, F. Biccari, F. Riboli, A. Gerardino, L. Li, E. H. Linfield, F. Pagliano, A. Fiore, and M. Gurioli, "Generalized fano lineshapes reveal exceptional points in photonic molecules," Nat. Commun. **9**(1), 396 (2018).
22. H. Haus, W. Huang, S. Kawakami, and N. Whitaker, "Coupled-mode theory of optical waveguides," J. Lightwave Technol. **5**(1), 16–23 (1987).
23. H. A. Haus and W. Huang, "Coupled-mode theory," Proc. IEEE **79**(10), 1505–1518 (1991).
24. W.-P. Huang, "Coupled-mode theory for optical waveguides: an overview," J. Opt. Soc. Am. A **11**(3), 963–983 (1994).
25. D. Rowland and J. Love, "Evanescent wave coupling of whispering gallery modes of a dielectric cylinder," IEE Proc.-J: Optoelectron. **140**(3), 177–188 (1993).
26. B. Little, S. Chu, H. Haus, J. Foresi, and J.-P. Laine, "Microring resonator channel dropping filters," J. Lightwave Technol. **15**(6), 998–1005 (1997).
27. C. Manolatou, M. J. Khan, S. Fan, P. R. Villeneuve, H. A. Haus, and J. D. Joannopoulos, "Coupling of modes analysis of resonant channel add-drop filters," IEEE J. Quantum Electron. **35**(9), 1322–1331 (1999).
28. S. Fan, W. Suh, and J. D. Joannopoulos, "Temporal coupled-mode theory for the fano resonance in optical resonators," J. Opt. Soc. Am. A **20**(3), 569–572 (2003).
29. W. Suh, Z. Wang, and S. Fan, "Temporal coupled-mode theory and the presence of non-orthogonal modes in lossless multimode cavities," IEEE J. Quantum Electron. **40**(10), 1511–1518 (2004).

Optics EXPRESS

30. Q. Li, T. Wang, Y. Su, M. Yan, and M. Qiu, "Coupled mode theory analysis of mode-splitting in coupled cavity system," Opt. Express **18**(8), 8367–8382 (2010).
31. M. Cai, O. Painter, and K. J. Vahala, "Observation of critical coupling in a fiber taper to a silica-microsphere whispering-gallery mode system," Phys. Rev. Lett. **85**(1), 74–77 (2000).
32. J. Kullig and J. Wiersig, "High-order exceptional points of counterpropagating waves in weakly deformed microdisk cavities," Phys. Rev. A **100**(4), 043837 (2019).
33. M. Bosch, S. Malzard, M. Hentschel, and H. Schomerus, "Non-hermitian defect states from lifetime differences," Phys. Rev. A **100**(6), 063801 (2019).
34. X. Zhang, K. Ding, X. Zhou, J. Xu, and D. Jin, "Experimental observation of an exceptional surface in synthetic dimensions with magnon polaritons," Phys. Rev. Lett. **123**(23), 237202 (2019).
35. X. Xue, X. Zheng, and B. Zhou, "Super-efficient temporal solitons in mutually coupled optical cavities," Nat. Photonics **13**(9), 616–622 (2019).
36. J. Wiersig, "Formation of long-lived, scarlike modes near avoided resonance crossings in optical microcavities," Phys. Rev. Lett. **97**(25), 253901 (2006).
37. H. Schomerus and J. Wiersig, "Non-hermitian-transport effects in coupled-resonator optical waveguides," Phys. Rev. A **90**(5), 053819 (2014).
38. S. Longhi, D. Gatti, and G. Della Valle, "Non-hermitian transparency and one-way transport in low-dimensional lattices by an imaginary gauge field," Phys. Rev. B **92**(9), 094204 (2015).
39. L. Du, Y. Zhang, and J.-H. Wu, "Controllable unidirectional transport and light trapping using a one-dimensional lattice with non-hermitian coupling," Sci. Rep. **10**(1), 1113 (2020).
40. S. Buddhiraju, W. Li, and S. Fan, "Photonic refrigeration from time-modulated thermal emission," Phys. Rev. Lett. **124**(7), 077402 (2020).
41. K. X. Wang, "Time-reversal symmetry in temporal coupled-mode theory and nonreciprocal device applications," Opt. Lett. **43**(22), 5623–5626 (2018).
42. Z. Zhao, C. Guo, and S. Fan, "Connection of temporal coupled-mode-theory formalisms for a resonant optical system and its time-reversal conjugate," Phys. Rev. A **99**(3), 033839 (2019).
43. B. Wu, B. Wu, J. Xu, J. Xiao, and Y. Chen, "Coupled mode theory in non-hermitian optical cavities," Opt. Express **24**(15), 16566–16573 (2016).
44. B. Zhen, C. W. Hsu, Y. Igarashi, L. Lu, I. Kaminer, A. Pick, S.-L. Chua, J. D. Joannopoulos, and M. Soljačić, "Spawning rings of exceptional points out of dirac cones," Nature **525**(7569), 354–358 (2015).
45. J. Wiersig, "Boundary element method for resonances in dielectric microcavities," J. Opt. A: Pure Appl. Opt. **5**(1), 53–60 (2003).
46. J. Ryu, S. Gwak, J. Kim, H.-H. Yu, J.-H. Kim, J.-W. Lee, C.-H. Yi, and C.-M. Kim, "Hybridization of different types of exceptional points," Photonics Res. **7**(12), 1473–1478 (2019).
47. J.-W. Ryu, S.-Y. Lee, and S. W. Kim, "Coupled nonidentical microdisks: Avoided crossing of energy levels and unidirectional far-field emission," Phys. Rev. A **79**(5), 053858 (2009).
48. T. Kato, *Perturbation theory for linear operators* (Springer, 1966).
49. W. D. Heiss, "Repulsion of resonance states and exceptional points," Phys. Rev. E **61**(1), 929–932 (2000).
50. H. A. Haus, *Waves and fields in optoelectronics*. (Prentice-Hall, 1984).
51. M. G. Raymer, "Quantum theory of light in a dispersive structured linear dielectric: a macroscopic hamiltonian tutorial treatment," J. Mod. Opt. **67**(3), 196–212 (2020).
52. A. V. Kanaev, V. N. Astratov, and W. Cai, "Optical coupling at a distance between detuned spherical cavities," Appl. Phys. Lett. **88**(11), 111111 (2006).
53. J.-W. Ryu, S.-Y. Lee, C.-M. Kim, and Y.-J. Park, "Directional interacting whispering-gallery modes in coupled dielectric microdisks," Phys. Rev. A **74**(1), 013804 (2006).
54. F.-J. Shu, C.-L. Zou, W.-C. Chen, and F.-W. Sun, "Ultralong distance coupling between deformed circular microcavities," J. Opt. Soc. Am. B **31**(3), 478–483 (2014).
55. J. Okołowicz, M. Płoszajczak, and I. Rotter, "Dynamics of quantum systems embedded in a continuum," Phys. Rep. **374**(4-5), 271–383 (2003).
56. M. Hentschel, "Optical microcavities as quantum-chaotic model systems: Openness makes the difference," Adv. Solid State Phys. **48**, 293–304 (2009).